Pergamon

Cement and Concrete Research 31 (2001) 1385–1392

CEMENT AND CONCRETE RESEARCH

A fractal study of the fracture surfaces of cement pastes and mortars using a stereoscopic SEM method

Yuting Wang[1], Sidney Diamond*

School of Civil Engineering, Purdue University, West Lafayette, IN 47907-1284, USA

Received 2 August 1999; accepted 25 June 2001

Abstract

A stereoscopic scanning electron microscopic (SEM) method, based on surface areas tallied over a much wider range of measurement scales than has been used in the past, was used to evaluate the fractal characteristics of fracture surfaces of cement pastes and mortars. Fracture surfaces of cement pastes exhibit two distinct fractal regimes: a regime of low fractal dimension (ca. 2.02) at low magnification scales and a significantly higher fractal dimension (ca. 2.12) at higher magnifications. The crossover occurs at a scale dimension slightly greater than 1 μm^2. Neither water/binder (w/b) ratio nor the presence of silica fume appears to influence these fractal characteristics. Cement paste areas exposed on mortar fracture surfaces are identical with those of cement paste specimens. In contrast to the paste areas, areas of crushed sand exposed on mortar fracture surfaces display a single fractal domain of significantly higher fractal dimension, around 2.20.

Keywords: Fractal; Fracture surfaces; Cement paste; Stereoscopic; Scanning electron microscopy

1. Introduction

As originally defined by Mandelbrot [1], the term "fractal" is a characteristic description applied to any boundary (in two dimensions) or to any bounding surface (in three dimensions) that remains self similar as the scale of examination is magnified (Fig. 1). The governing characteristic of fractal boundaries is not the roughness of the boundary, but the self-similarity, i.e., that the geometry of the boundary appears identical at any degree of magnification.

Fractal boundaries may exhibit various degrees of convolution, so long as the boundary is equally convoluted at all scales. The degree of convolution is expressed in terms of a "fractal dimension." Fig. 1, after Russ [2], gives a graphic example of the appearance on a plane of bounding surfaces of several different fractal dimensions.

Self-similarity necessarily implies that the apparent or measured length of the boundary (or apparent or measured area of the bounding surface) increases with magnification, or as the size of the measurement scale used to measure the boundary length is reduced. Specifically, the total length (L) of a fractal boundary that is measured using a particular measuring scale length (η) is taken as (Eq. (1)):

$$L = L_o \eta^{-(D_F - D)} \tag{1}$$

where L_o is a constant, D_F is the fractal dimension, and D is the relevant topological dimension, i.e., 1 for a bounding line on a two-dimensional surface. Thus, for a fractal line boundary, a log–log plot of total measured perimeter lengths compiled using progressively decreasing measurement scales (i.e., decreasing ruler lengths) vs. ruler length produces a straight line with a negative slope $-(D_F - D)$. A similar equation can be written for a fractal bounding surface in three dimensions; here, the topological dimension is 2.

In many real three-dimensional fractal systems, a distinction is made between "true" self-similar systems, which are self similar in all directions in the same manner, and so-called "self affine" systems, where the scaling is not the same in the x, y, and z directions. Fracture surfaces of solids necessarily fall into this category since such fractal surfaces are necessarily constrained differently in the z direction, by virtue of being a surface.

* Corresponding author. Tel.: +1-765-494-5016; fax: +1-765-496-1364.

E-mail address: diamond@ecn.purdue.edu (S. Diamond).

[1] Present address: The Face Companies, 427 West 35th Street, Norfolk, VA 23508, USA.

0008-8846/01/$ – see front matter
PII: S0008-8846(01)00591-9

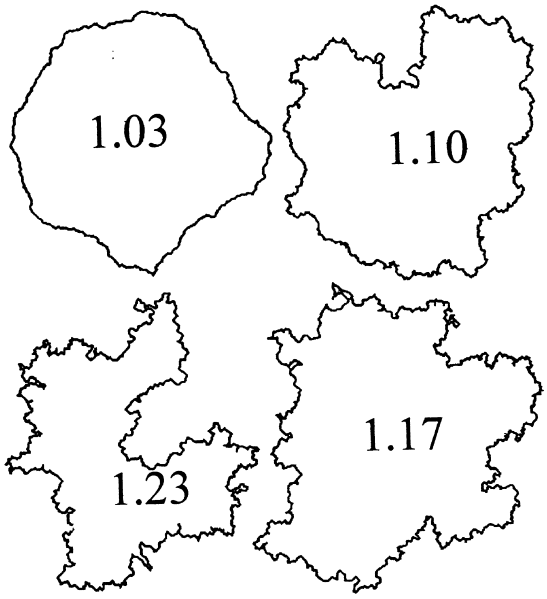

Fig. 1. Fractal boundaries of varying fractal dimension varying from 1.03 (upper left) to 1.23 (lower left).

Two other parameters are important in describing a real, as distinguished from a mathematical fractal system. Since real fractal systems cannot be self similar at all possible measurement scales, there are necessarily lower and upper boundaries to the scale range within which they exist. The values of η that constitute the lower and upper limits of this range are important descriptors of the system. The lower limit can be no smaller than the atomic size range. The upper limit may or may not approach the size of the body being described. In most practical applications of the fractal concept, the size ranges that can be examined are set by the instrumentation used, and the true limits are not evaluated.

It should also be pointed out that a particular system may exhibit different fractal structures at different scales, or that it may be fractal over some range of scales and not fractal at others. For example, it has been shown [3] that many microporous materials exhibit fractal characteristics at small length scales but are not fractal at large scales. Conversely, aggregations of smooth-surface particles may be fractal at large scales but not fractal at scales approaching that of the smooth-surface particles. Fig. 2, taken from Ref. [4], shows a case where two different fractal regimes and a nonfractal regime occur at different length scales. The figure shows the fractal plot for the boundary of the projection on a plane of an agglomeration of smooth-surface spheres. The straight-line segment at large measurement scales is a fractal descriptive of the gross rugged surface structure of the agglomerate, here of fractal dimension 1.22. The second straight-line region at intermediate scales represents the fine texture of the bounding surface of the agglomeration, showing a fractal dimension of 1.15. The flat portion of the plot indicates that at a fine scale commensurate with that of the smooth surfaces of the individual particles, the boundary of the agglomeration is not fractal.

In this paper, we report results of investigations into the fractal character of fracture surfaces of cement pastes and of mortars, over a very wide range of size scales.

2. Previously reported measurements

Fractal analysis has been attempted for a variety of fracture surfaces of concretes and cement pastes by several researchers. A variety of techniques have been used, with varying results.

Using a profilometer, Saouma and Barton [5] studied the profiles of fracture surfaces of concrete, and reported that they are fractal and that the profiles have fractal dimension values between 1.06 and 1.12 over the measured range of scales. These profile fractal dimensions correspond to surface fractal dimensions of between 2.06 and 2.12.

Issa and Hammad [6] also attempted to measure concrete fracture surface fractal dimensions, using a modified slit-island method and, separately, a two-dimensional Fourier spectral method. Their results for both methods were higher than those of other investigators, being about 2.21 for the slit-island method and a very high value of 2.59 for the Fourier method.

Lange et al. [7] measured fracture surface fractal dimensions of cement pastes and mortars using a confocal microscopic method. They obtained fracture surface fractal dimensions around 2.10, similar to those obtained by Saouma and Barton [5].

More recently, Chiaia et al. [8] carried out fractal analyses of cracks induced in several concretes by applying a splitting load to notched thin plate specimens. Using a box-counting method, they measured fractal dimensions between 1.03 and 1.25, depending on the nature of the

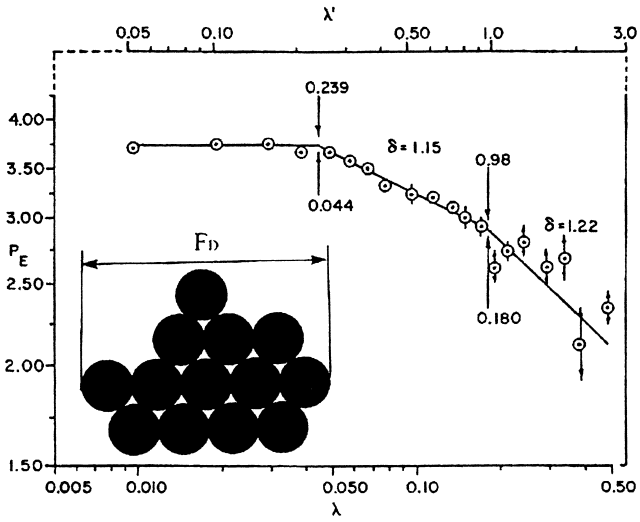

Fig. 2. Fractal plot for an agglomeration of smooth-surface spheres. P_E, the perimeter length, and λ, the stride length, are both normalized with respect to Feret's diameter. The top scale, λ', is normalized with respect to the sphere diameter (after Kaye [4]).

concrete, and on whether the fractal dimension was measured for bond cracks around the aggregates or for the geometrically more complex (and higher fractal dimension) bond cracks. The corresponding surface fractal dimension range would be 2.03–2.25.

3. Methods of surface fractal dimension measurement

As indicated by the brief survey above, various methods can be used for determining the fractal dimension of a rough surface such as that produced by the fracture of concrete or cement paste. They vary in reliability, experimental convenience, and importantly, in range of sizes that can be observed.

The "direct" method for measuring a surface fractal dimension of a fracture surface is to measure surface area over a wide range of characteristic scales. This is extremely difficult to do on a cement paste or concrete fracture surface, and most workers have resorted to various indirect methods. The exception is Lange et al.'s [7] surface area measurements using a confocal microscope; unfortunately, they were able to explore only a very limited range of size scales.

Various indirect methods exist. A common indirect method often used in metallurgy is the vertical section method [9,10], in which sections perpendicular to the fracture surface are sliced and one-dimensional profiles of the fracture surface are generated from these sections and evaluated; Saouma and Barton [5] used this method. Box-counting methods applied to traces of the fracture crack appearing on planar surfaces, such as that used by Chiaia et al. [8], are sometimes used. The slit-island method, a variant of which was employed by Issa and Hammad [6], is sometimes used. In this method, the specimen is repeatedly polished parallel to the fracture surface. "Islands" appear on the fracture surface during polishing and grow in size as polishing is continued. The fractal dimension is calculated from the slope of the log of the perimeter of these islands vs. the log of their area.

Some years ago, a direct method involving actually measuring the surface area of the true fracture surface over a large range of size scales was described by Friel and Pande [11]. This procedure employed a stereoscopic application of scanning electron microscopy (SEM), using stereo pairs obtained at various magnifications. In the procedure, arrays of points are placed on the surface of the stereo image by the computer, each point occupying its individual elevation above a reference plane. Triangles, tilted at various angles in three-dimensional space, are generated by connecting adjacent points in the array. The area of each triangle is measured, and the indicated surface area is the sum of the areas of all of these triangles. The measurement scale can be changed by varying the magnification, and within a given magnification, by changing the density of the array of points on the surface. The fractal dimension is obtained from the relationship between the log of the measured surface area and the log of the measurement scale.

The method is experimentally very demanding, and because of this has not been much used. However, a program to execute such measurements is commercially available, and was supplied by PGT as part of the IMIX system used with our SEM.

In the present study, we have applied this method for direct measurement of the fractal dimensions of fracture surfaces of mortars and of cement pastes over a wide range of size scales. In the mortar studies, we have made separate measurements of the portion of the fracture surface consisting of cement paste and that portion consisting of sand grains; the two types of surface element were shown to have quite different fractal characteristics. This distinction appears not to have been made previously.

4. Details of the stereoscopic SEM method used

The fundamental tenet of the method is that if the heights of *all* points on the fracture surface above a base reference plane can be established, its true surface area can be measured. If the heights of a dense network of points (but not all points) can be established, the true surface area can be approximated. The less dense the network of points whose height is established, the less accurately the individual convolutions are mirrored, and the smaller is the measured surface area. Furthermore, at lower magnification, fewer details of the fracture surface are resolved in the image, and again, the indicated surface area is smaller. The relationship between the reduction in measured surface area and the decrease in measuring increment (due to the effects of the combination of reduced magnification and decreased space between measured points) provides the basic information from which the inherent fractal dimension of the surface can be calculated.

In the measurement, a grid of points is placed on the rough fracture surface, from which the surface is "profiled" by subdividing it into an array of triangular cells tilted at various angles to each other. The elevation of the boundary points of each triangular cell is established by stereoscopic means, the details of which are discussed later. Each triangle is thus positioned accurately in three-dimensional space and the sum of the areas of all of the triangles can be evaluated. The calculated area of this profiled surface conforms to the true fracture surface area to some limited degree of approximation. The degree of approximation increases with increasing magnification and with increasing density of points making up the grid.

In this study, the grid density was varied from 10×10 (100 points) to 70×70 (4900 points) at each magnification level used. Six levels of magnification were used, specifically $\times 50$, $\times 100$, $\times 500$, $\times 1000$, $\times 5000$, and $\times 10{,}000$. As indicated in Table 1, for each combination of magnification and grid point density, a measurement scale area exists

Table 1
Measurement scale areas (in μm^2) as functions of magnification and grid point density

Magnification	10×10	20×20	40×40	50×50	70×70
$\times 50$	26,010	5831	1385	877	442
$\times 100$	6119	1372	326	206	104
$\times 500$	267	60	14.2	8.98	4.53
$\times 1000$	69.5	15.6	3.7	2.34	1.18
$\times 5000$	2.82	0.63	0.15	0.095	0.0479
$\times 10{,}000$	0.69	0.155	0.0368	0.0233	0.0117

in terms of fractal analysis. This is the area of a unit triangle, as taken on a flat plane. The area of this characteristic two-dimensional "measuring stick" varied over six orders of magnitude, between 2.6×10^4 and 0.01 μm^2.

The stereometric measurement of the elevation of each grid point employed the geometry indicated in Fig. 3 (after Friel and Pande [11]).

The equation used to calculate the height of any given grid point on the surface above a reference plane is:

$$Z = \Delta x / 2\sin(\alpha/2) \tag{2}$$

where Z is the height of the point above the reference plane, α is the parallax angle (i.e., the tilt angle between the left and right stereoscopic images), and Δx is the displacement in the x direction between the left and right images. In the implementation used, the parallax angle was set by the operator at 6°. The displacement in the x direction was calculated by measuring the separation distance between the corresponding pixels in the left and right images. The corresponding pixels in the two images are identified by a template-matching algorithm on the basis of brightness patterns. The heights of each of the grid points was calculated by Eq. (2).

After calculating the measured approximation to the true surface at each specified magnification and density of grid points, an adjustment is needed to account for the fact that the electron beam rasters over progressively smaller areas at progressively larger magnifications. In this study, the areas measured at each magnification other than $\times 100$ were multiplied by the appropriate factor to bring them to what they would have been if measured at $\times 100$.

In the final step, the measured or "profiled" surface areas (adjusted for raster scan area) were plotted against the measurement scales on a log–log plot, and the fractal dimension was calculated from the slope of the plot. The equation used for the final calculation, as indicated by Friel and Pande [11] and by Underwood and Banerji [12] is (Eq. (3)):

$$\log S = \log S_o - \frac{1}{2}(D_F - 2)\log(\eta^2) \tag{3}$$

where S is the profiled surface area, S_o is a constant, D_F is the indicated fractal dimension, and η^2 is the characteristic measurement scale area.

5. Materials studied and sample preparation

Most of the specimens investigated in this study were mortar and cement paste specimens from previous research reported by Diamond and Mindess [13]. An ordinary portland cement (OPC) used in producing these, a commercial naphthalene sulfonate superplasticizer, and silica fume in powder form were incorporated in some of the mixes. The water/binder ratios (w/b) were 0.30 and 0.50. The mortars and cement pastes were each mixed using the appropriate ASTM C 305 procedures. The mixes were then cast in 42-mm diameter, 168-mm length cylinder specimens with provision for a chevron notch provided in accordance with the International Rock Mechanics Association Method 1. They were cured in a fog room for 24 h, demolded, and cured in lime-saturated water for 3 weeks prior to being subject to controlled fracture. Two sands were used in the mortars, both being manufactured sand prepared from rock samples. The rocks were, respectively, an andesite and a dolomite. In both cases, the maximum particle size was 4.8 mm and the mean size was about 1 mm after crushing. The fineness moduli for the two sand were 3.01 for the andesite sand and 2.96 for the dolomite sand. The sand/cementitious materials ratio of the mortars was 2.0.

The fracture process for both cement pastes and mortars involved third-point loading of the notched beams in flexure, with repeated loading and unloading cycles being carried out until failure. SEM specimens were then prepared from the fracture surfaces thus obtained, and the surfaces were coated with gold–palladium alloy in the normal manner.

In addition to the specimens described above, a 23-year-old cement paste specimen (designated specimen H) was also examined. This specimen was simply fractured with a chisel.

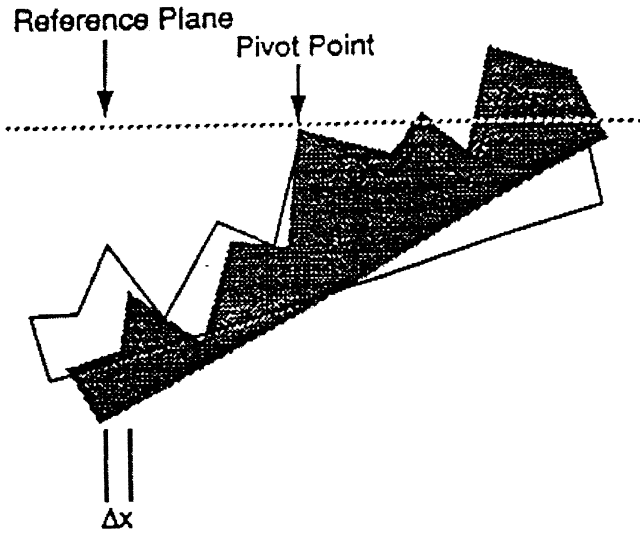

Fig. 3. Diagram showing a schematic fracture surface at two tilt angles.

Table 2
Mix proportions for the cement pastes and mortars used

	Mix proportions (by weight) and other details				
Specimen code	Cement	SF	Water	Naphthalene sulfonate dosage (%)[a]	Aggregate used
OPC 0.5	1	–	0.5	–	none
OPC + SF 0.5	0.85	0.15	0.5	–	none
OPC + SF 0.3	0.85	0.15	0.3	2	none
H	1	–	0.4	–	none
NA	1	–	0.3	1	andesite
ND	1	–	0.3	1	dolomite
HD	0.85	0.15	0.3	2	dolomite

[a] Naphthalene sulfate dosage in percentage by weight of cement + silica fume.

Table 2 describes the specific specimens studied in the fracture surface fractal analysis.

6. Results

The results of fractal dimension measurements of the fracture surfaces of cement pastes and of the aggregates in mortars are provided in Table 3. In each of these determinations, five separate regions on the fracture surfaces were examined for each specimen; the results provided are the average values obtained.

A number of typical fractal plots for the fracture surfaces of cement pastes are shown in Fig. 4a–d.

It is evident that these plots all fall clearly into two distinct linear regions with different slopes. The correlation coefficients within each region were in the range of .90–.99, and as evident in the figure, the data clearly describe two straight-line segments and not a curve.

We interpret this finding as indicating that cement paste fracture surfaces have two distinct ranges of fractal character, a coarse domain of modest rugosity and fractal dimension and a fine domain of significantly higher fractal dimension. The break point between the two regimes fluctuates slightly but is somewhere between 1 and 5 μm^2. This is roughly the size range of individual hydration product particles in hydrated cement systems.

In the coarse-resolution regime (of measurement scales between a little more than 1 and 10^4 μm^2), all of the cement paste fracture surfaces show a highly consistent fractal dimension, varying only between 2.02 and 2.04. In the fine-resolution regime (of characteristic scale area below ~ 1 μm^2), the fractal dimensions of the different cement pastes vary between 2.08 and 2.14, also not a wide range of variation.

The measured fractal dimensions of all of the samples studied are provided in Table 3.

In an early qualitative study of fracture surfaces of cement pastes using SEM stereo pairs, Diamond and Mindess [13] observed that self-similarity does not appear to hold for the entire range of magnifications examined. Instead, fracture surfaces of cement pastes appeared to reflect specific features dependent on the preexisting crystal or particle assemblages as exhibited at specific size scales. This observation is confirmed by the present study. The physical meaning of these findings can be illustrated by examination of Fig. 5a and b. This figure shows SEM micrographs of the same area of a cement paste fracture surface, taken at $\times 500$ and $\times 5000$, respectively, to illustrate the difference in appearance of the fracture surface in the two size ranges. The fractal dimensions exhibited at the lower magnification ranges are consistent with the relatively modest structural irregularities of the fracture surface. At higher resolution, the influence of inherent microstructural features of the cement paste, such as the fine pores and fine individual grains of hydration products, come into play. The fractal dimension reflects the finer textural details of the cement paste as exposed on the fracture surface.

The two distinct fractal regimes found on the fracture surface of cement pastes have their exact counterparts in the areas of cement paste that are exposed on the fracture surfaces of mortars. As indicated in Table 3, there seems to be no difference between the fractal characteristics of

Table 3
Measured fractal dimensions[a] for fracture surfaces of cement pastes, cement paste areas in mortars, and sand areas in mortars

Element measured	D_f	D_c	D_f	D_c	D_f	D_c	D_f	D_c	D_f	D_c	Average D_f	Average D_c
Paste OPC 0.5	2.11	2.02	2.14	2.02	2.12	2.03	2.12	2.04	2.10	2.03	2.12	2.03
Paste OPC + SF 0.5	2.10	2.02	2.13	2.02	2.10	2.01	2.14	2.03	2.09	2.02	2.11	2.02
Paste OPC + SF 0.3	2.10	2.02	2.11	2.02	2.09	2.02	2.10	2.02	2.12	2.02	2.10	2.02
Paste H	2.12	2.01	2.09	2.02	2.08	2.01	2.13	2.02	–	–	2.11	2.02
Paste in mortar NA	2.13	2.03	2.12	2.02	2.12	2.03	2.11	2.03	2.13	2.04	2.11	2.03
Paste in mortar ND	2.11	2.01	2.13	2.03	2.09	2.02	2.13	2.02	2.12	2.03	2.14	2.02
Paste in mortar HD	2.12	2.03	2.10	2.01	2.14	2.03	2.12	2.02	2.11	2.03	2.10	2.01
Andesite sand in mortar HA	2.22		2.34		2.22		2.18		–		2.24	
Dolomite sand in mortar ND	2.18		2.18		2.16		–		–		2.17	

[a] D_f and D_c are measured fractal dimensions in the fine and coarse regimes, respectively.

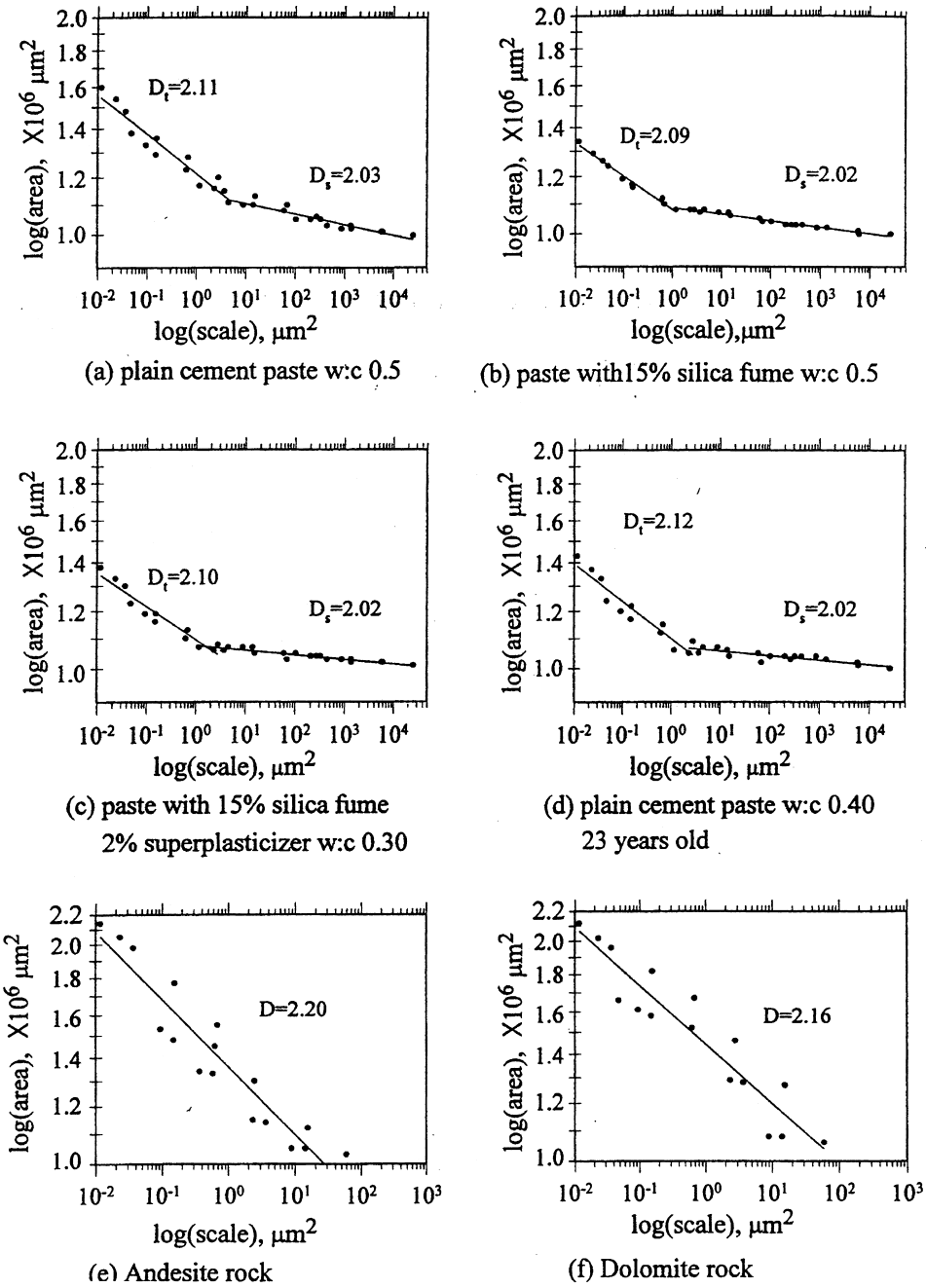

Fig. 4. Fractal plots of the fracture surfaces of cement pastes and aggregates.

cement paste specimens and of mortar specimens, as long as the analysis is confined to the cement paste portions of the mortar surfaces.

However, it was found that the fractal characteristics of sand grain areas exposed on mortar fracture surfaces are very different from the cement paste areas exposed on the same surfaces. Figs. 4e and 4f display typical fractal plots for sand found on the mortar fracture surfaces. To insure that the entire image was confined to a single sand grain, the lowest magnifications were not used in these determinations, the magnification range used being between $\times 500$ and $\times 10{,}000$. The variation in measurement scale from the 10×10-point grid at $\times 500$ magnification to the 70×70-point grid at $\times 10{,}000$ magnification is still four orders of magnitude. Within this range, the fractal plots for mortars of both the andesite and dolomite sands each show a single straight line, with correlation coefficient R^2 being about .94. Thus, only a single fractal regime seems to exist for sands on fracture surfaces, at least within the range of observation. The fractal dimension measured was in each case signifi-

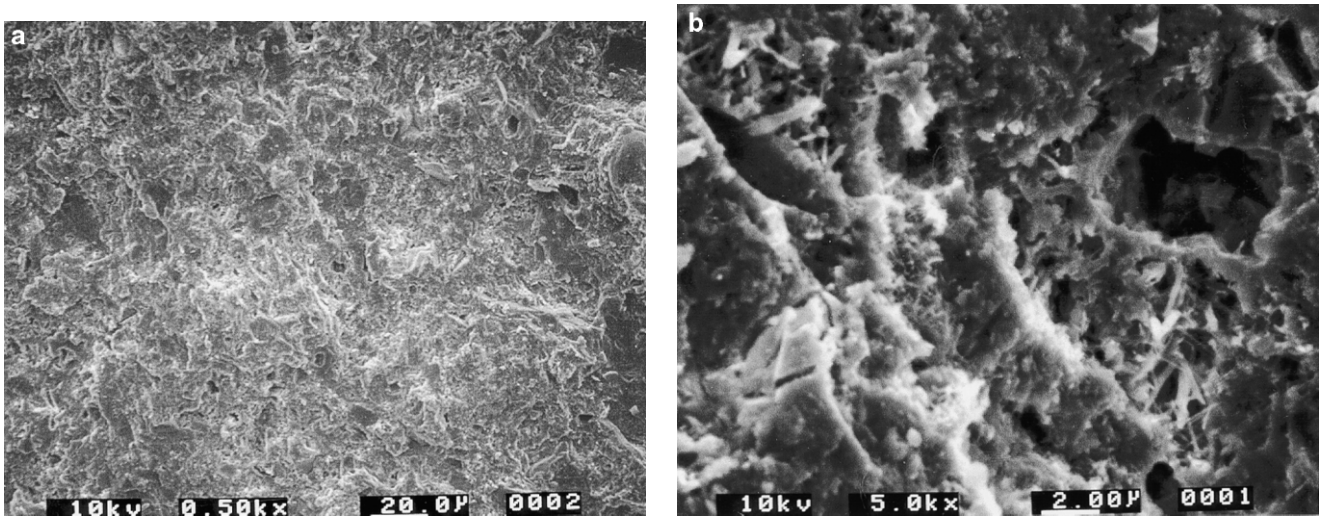

Fig. 5. (a) Area of cement paste fracture surface at $\times 500$. (b) Central portion of area above at $\times 5000$.

cantly greater than for the paste regions of the same fracture surfaces, averaging 2.24 and 2.17, respectively, for the andesite and dolomite sands as exposed on mortar surfaces.

7. Discussions

A significant finding of this study is that the fractal dimensions of the fracture surfaces of cement pastes of quite different characteristics are essentially the same. The presence or absence of silica fume and the variation in w/b do not seem to have much effect on the fractal dimension recorded either at high resolution or at low resolution. The high-resolution fractal dimensions were slightly more variable than those found in the low-resolution regimes, but even here, the fractal dimensions recorded varied only between 2.08 and 2.14 for pastes of w/b 0.3–0.5, with and without silica fume.

Another important finding is that the cement paste areas on the mortar fracture show the same surface fractal structures and dimensions as exhibited on fracture surfaces of plain cement pastes. This was not necessarily expected.

Still another unexpected finding is that the mode of generation of the fracture surface did not seem to be important. Cement paste "H," fractured with a hammer and chisel, showed the same fractal dimensions and characteristics as the fracture surfaces produced by repeated flexural loading.

The present results appear to mark the first-time fractal dimensions of cement paste areas in mortars and concretes have been compiled separately from those of aggregate areas on the same fracture surface. It appears to the writers that attempting to characterize the fracture surfaces of these composite materials without making such a discrimination involves mixing information of two separate kinds, and necessarily obscures the result.

The general range of fractal dimensions recorded in these studies is in fair agreement with those recorded in most of the previous studies cited. If a fracture surface is tallied without discrimination between the paste and aggregate components, one might expect some value intermediate between the two. None of the determinations previously cited from the literature extend to the high-resolution domain detected here. Accordingly, one might expect "blended" values intermediate between about 2.03 (the low-resolution value for cement pastes) and about 2.20 (the approximate value for aggregates). On a surface fractal basis, Saouma and Barton's [5] values ranged between 2.06 and 2.12, Lange et al.'s [7] were around 2.10, and those of Chiaia et al. [8] were between 2.03 and 2.25. The values obtained by Issa and Hammad [6] were somewhat higher, and their Fourier spectra method determination was especially high compared to the other measurements recorded.

The data recorded in the present work suggest that the fine-scale fractal characteristics of cement paste fracture surfaces are fairly robust from the scale of individual particles down to $\sim 0.01\ \mu m^2$. However, this fractal regime may not extend to the nanometer-size range characteristic of the finest internal structure of hydrated cement. Winslow et al. [14] made careful measurements of the fractal characteristics of the internal structure (not surface structure!) of cement pastes using small angle X-ray scattering. They found that over their "coarse" scale of 200–1500 Å (corresponding to the range 4×10^{-4} to $2 \times 10^{-2}\ \mu m^2$ in the area terms used in this paper), the fractal dimensions recorded were between 2.5 and 3.0, much higher than the surface fractals recorded here. The indication is that the internal "surface" structure giving rise to the X-ray scattering was exceedingly rough. For undried pastes, features on a still finer scale (below $4 \times 10^{-4}\ \mu m^2$) were found which were described as "mass fractals," i.e., of fractal dimension greater than 3. These mass fractal characteristics were, however, lost on drying.

8. Conclusions

1. It was found that cement paste fracture surfaces exhibited two distinct fractal regimes; a regime of modest fractal dimensions ($\sim$2.03) for higher measurement scales, and a regime of significantly higher fractal dimensions ($\sim$2.10–2.13) for finer measurement scales. The finer measurement scales extended down to scales of the order of 0.01 μm^2.

2. The two fractal regimes intersect at a measurement scale between approximately 1 and 5 μm^2, the size range for most C-S-H gel particles.

3. The values were independent of w/b (within the range of 0.3–0.5), and of whether or not the pastes incorporated silica fume and superplasticizer.

4. Cement paste fracture surfaces produced by hand cleaving showed fractal dimensions essentially identical to those of fracture surfaces generated by repeated bending of the notched specimens.

5. Cement paste areas exposed on fracture surfaces of mortar specimens showed fractal characteristics essentially identical to those measured on fracture surfaces of separate cement paste specimens.

6. Fractal characteristics measured for manufactured sand grains exposed on mortar fracture surfaces were considerably different than for cement paste areas exposed on the same surfaces. Data for all size ranges examined fell on a common straight line indicating a single fractal dimension characterized the sands. The fractal dimensions recorded for the two types of manufactured sand used were both on the order of 2.2, significantly higher than the fractal dimensions of the cement paste on the same fracture surfaces.

7. It appears that previous determinations of fractal dimensions of cement pastes by others were carried out over measurement scales too coarse to detect the transition between the two cement paste fractal regimes detected in this work. Nevertheless, the range of values reported by others for mortars are seemingly consistent with the idea that they represent blended fractal dimensions reflecting separate contributions from cement paste and aggregate.

Acknowledgments

The material presented here was derived from the PhD thesis of the first-named author. The support of the National Science and Foundation Science and Technology Center for Advanced Cement-Based Materials is gratefully acknowledged.

References

[1] B.B. Mandelbrot, The Fractal Geometry of Nature, Freeman, New York, 1982.
[2] J.C. Russ, Fractal Surfaces, Plenum, New York, 1994.
[3] D. Avnir, D. Farin, P. Pfeifer, Molecular fractal surfaces, Nature 308 (1984) 261–263.
[4] B.H. Kaye, The description of two-dimensional rugged boundaries in fine particle science by means of fractal dimensions, Powder Technol. 46 (1986) 245–254.
[5] V.E. Saouma, C.C. Barton, Fractals, fractures, and size effects in concrete, J. Eng. Mech. 120 (1994) 835–854.
[6] M.A. Issa, A.M. Hammad, Assessment and evaluation of fractal dimension of concrete fracture surface digitized images, Cem. Concr. Res. 24 (1994) 325–334.
[7] D. Lange, H. Jennings, S.P. Shah, Relationship between microstructure, fracture surfaces and material properties of portland cement, J. Am. Ceram. Soc. 76 (1993) 589–597.
[8] B. Chiaia, J.G.M. van Mier, A. Vervuit, Crack growth mechanism in four different concretes: Microscopic observation and fractal analysis, Cem. Concr. Res. 28 (1998) 103–114.
[9] C.S. Pande, L.E. Richards, N. Louat, B.D. Dempsey, A.J. Schwoeble, Fractal characterization of fracture surfaces, Acta Metall. 35 (1987) 1633–1637.
[10] F.E. Underwood, K. Banerji, Fractals in fractography, Mater. Sci. Eng. 80 (1986) 1–4.
[11] J.J. Friel, C.S. Pande, Direct determination of fractal dimensions of fractured surfaces using scanning electron microscopy and stereoscopy, J. Mater. Res. 8 (1993) 100–104.
[12] E.E. Underwood, K. Banerji, Metals Handbook, ninth ed., vol. 12, ASM International, Materials Park, OH, 9193-210, 1988.
[13] S. Diamond, S. Mindess, SEM investigations of fracture surfaces using stereo pairs: I. Fracture surfaces of rock and of cement paste, Cem. Concr. Res. 22 (1992) 67–78.
[14] D.N. Winslow, J.M. Bukowski, J.F. Young, The fractal arrangement of hydrated cement pastes, Cem. Concr. Res. 25 (1995) 147–156.